Detecting High-Frequency Gravitational Waves With the Pulsar Timing Array

Daniel Halmrast
Advisor: Timothy Dolch

Abstract

Multiple-hour long observations of single pulsars allow us to probe relatively high-frequency regions of the gravitational wave (GW) spectrum typically outside the sensitivity of the pulsar timing array (PTA). Using such single pulsar observations from the North American Nanohertz Observatory for Gravitational Waves (NANOGrav), we applied known techniques for seeking single-source continuous wave (CW) sources. By analyzing simulated data with an injected source, we verified the accuracy of the CW search method for hours-long data sets. Furthermore, by applying an identical analysis to the true data, we found that the data places new upper limits on GW strain in the high frequency regime.

1 Introduction

The search for low-frequency GWs in the universe is currently best carried out using Pulsar Timing Arrays (PTAs). The incredible precision timing of pulsars, along with their relative abundance in the universe, makes the PTA a high precision gravitational wave detection instrument with the ability to probe a large range of the gravitational wave parameter space.

The sensitivity of the PTA is due to two factors: the natural precision of millisecond pulsars, and the self-correcting nature of the timing model used to model pulsar behavior. Both of these aspects of the PTA will be covered in more detail in the next section.

The high fidelity of the PTA stems mainly from the fact that there is an abundance of pulsars in the galaxy with many different sky locations.

Each line-of-sight to a pulsar provides data on the strength of GWs from any GW sources in the same direction as the pulsar. Furthermore, each pair of pulsars provides correlation data that can give additional information about GWs. This is because each line-of-sight gives information analogous to the projection of the wave onto the line-of-sight. Thus, to ascertain a two-dimensional signal source position, at least two lines of sight are needed. Furthermore, with additional lines of sight, correlation restrictions can be put on the data to add to the confidence of a detection.

For example, if the data from two lines of sight suggested a source location at some coordinates (θ, ϕ), one would expect any other set of two lines of sight to yield the same result. If a second set of lines of sight confirmed that the source location was at coordinates (θ, ϕ), that would add to the confidence of the detection. However, if another line-of-sight were to predict different coordinates, that would suggest that the (θ, ϕ) detection in the first pair of pulsars is more likely to be a false positive.

With so many lines of sight, many interesting properties of GWs can be probed, including precise measurements of the location of the source, as well as the strain of the gravitational wave itself. However, the hallmark of such a detector is the ability to detect the stochastic background of GWs. This is described in further detail in the next section.

2 Background

The goal of this section is to provide a comprehensive background of the theory and techniques used in gravitational wave pulsar astrophysics.

It is necessary, then, to first understand what a pulsar is. When a massive star reaches the end of its life cycle, it has the potential to end its life as a supernova. This occurs when the core of the star runs out of material to fuse, and the fusion reactions begin to slow down. As the rate of fusion decreases, the outward pressure caused by the fusion also decreases. There reaches a point, then, when the pressure due to fusion does not balance the gravitational pressure of the star. At that point, the star collapses on itself in a catastrophic event. After such an event, there are a few possibilities for the outcome of the core remnants of the star. If the gravitational pressure is enough to force the core past its Schwarzschild radius ($r \leq \frac{2Gm}{c^2}$), the core will collapse into a black hole. On the other hand, if the gravitational pressure is relatively weak, the core will remain relatively undisturbed, and

will become a white dwarf star. In the intermediary range between these two possibilities lies a third one; if the gravitational pressure is just barely not enough to force the core into a black hole state, it will instead force the formation of a neutron star. Neutron stars are the most extreme objects in the universe after black holes. With such intense gravitational forces forming them, high-energy nuclear processes occur in the atoms that formed the core of the original star. As protons and electrons are pushed together, it becomes energetically favorable for the electrons to undergo reverse beta decay, and fuse into neutrons. With no electrostatic repulsion between the protons and electrons, the core mass–which is almost all neutrons at this point–can collapse further on itself, achieving a density similar to that of an atomic nucleus. At this point, the core mass has reached a stable configuration, and is now a neutron star. Approximately 1.4 solar masses of core material forms the star, which is spherical with a diameter of about 10 km.

After the formation of the neutron star, there is a possibility that the star will be "spun up" to high angular speeds. If the star was in a binary system, it may accrete material from its companion, and acquire angular momentum from it. Since the neutron star has such a small radius, a small change in angular momentum will be magnified to a larger change in the angular velocity of the star.

Another peculiar feature of neutron stars is their intense magnetic fields–up to 10^8 times as much as the earth. For neutron stars that are spinning rapidly, this magnetic field moves very rapidly through space, and it is thought that the accelerating free electrons emit synchrotron radiation, which is then forced out of the poles of the magnetic fields in a beam formation.

A pulsar is exactly this sort of object: a rotating neutron star with beam emissions of electromagnetic waves. Pulsars are particularly bright in radio frequencies, which makes them well-suited for study using radio telescopes. They have very slow spin-down rates, so their periods are very stable in time. A common way to represent this is through a $P - \dot{P}$ diagram. These diagrams plot the spindown rate ($\dot{P}$) versus the period of the pulsar (P). As seen in the $P - \dot{P}$ diagram for the known pulsars of the galaxy (Figure 1), there exists a certain class of pulsars with incredibly low periods and spin-down rates. These are known as the millisecond pulsars, called such due to their extremely fast rotational periods. With such amazing stability and cadence, millisecond pulsars function incredibly well as stellar timekeepers, with some rivaling even an atomic clock's precision. It is this stability that

makes millisecond pulsars the primary data source for gravitational wave searches with pulsars.

A gravitational wave is a perturbation in spacetime caused by a rotating mass quadrupole moment somewhere in the universe. The most common sources of gravitational waves are black hole binary systems, especially supermassive (10^9 solar masses or more) black hole binaries that occur in association with galaxy collisions. Such binary systems emit sinusoidal GWs that give rise to the perturbation. This perturbation occurs in the local metric of the space, and represents a change in the space-time intervals between objects. The co-ordinate distances remain fixed, but the practical (e.g. light travel time) distance is perturbed slightly.

The Laser Interferometer Gravitational-Wave Observatory (LIGO) detectors recently announced the first detection of gravitational waves [4]. The experiment detected a strain $\frac{\delta L}{L} \approx 10^{-21}$, corresponding to an absolute distance change on the order of a fraction of a proton diameter. The LIGO observatory was able to detect such small changes in distance by using an optimized interferometer. By splitting a laser along two orthogonal paths, reflecting them back to each other, and observing the interference magnitude, an interferometer is able to precisely measure extremely small changes in the differential lengths of their arms. One way of conceptualizing the interferometer is by following the peaks (highest electric field magnitude) of the light emitted by the laser across the device. The peaks are evenly spaced in the arm, and without loss of generality will recombine constructively. However, imagine a change in the length of one of the arms. Now, the peaks along one arm have more distance to travel, and thus will arrive delayed compared to their companions. Such a delay will induce a slightly destructive interference in the resulting recombination beam, and will be detectable by a light intensity detector. One can think of the stable arm as a "reference beam", and the changing arm as the "detector beam". With this mode of thinking, the interferometer acts as a comparison device between the reference beam and the detector beam.

In a way, pulsar timing functions the same way as interferometers do. The line-of-sight between us and the pulsar functions as the detector beam, with the pulses originating from the pulsar functioning as the crests. In order to get the equivalent of a reference beam, it is necessary to develop a timing model that describes with great precision the expected time of arrival of the pulse from the pulsar. With such a timing model, it is possible to compare the measured time of arrival and the expected time of arrival to

Figure 1: The $P - \dot{P}$ diagram [7]. Here rotational periods (x-axis) are plotted against their spindown rates. Millisecond pulsars live in the bottom left quadrant of the plot, and spin down very slowly.

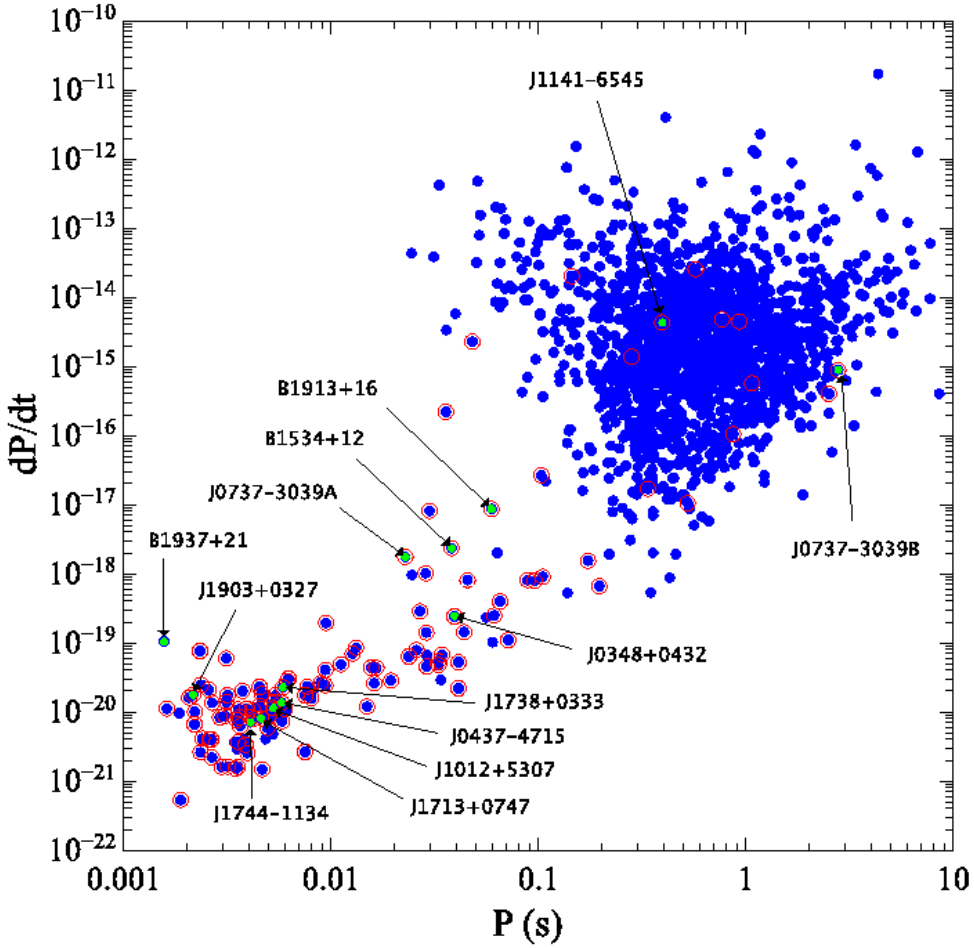

gain information about the distance changes along the line-of-sight of the pulsar.

However, such a method requires an incredibly accurate timing model for the pulsar that takes into account all known effects between the earth and the pulsar. Such a model has been developed, and is used in the analysis pipeline to accurately calculate the expected time of arrival of a pulse. The timing model takes into account a wide array of effects. First and foremost, the timing model requires a precise measurement of the period of the observed pulsar, as well as the spindown rate, to model the pulse source accurately. Next, the timing model takes into account the motion of the earth relative to the pulsar. The model normalizes the times of arrival to the center of the solar system, and accounts for the movement of the pulsar towards, away, or transverse to the solar system. Next, the model takes into account any effects due to general relativity, including the Shapiro delay effect for binary systems, and precession for orbiting pulsars. The Shapiro delay is a time dilation in a pulsar's pulsation rate when those pulses pass near a massive object (in this case, the object being the pulsar's binary companion).

The ultimate goal of the timing model is to "zero out" any known effects between us and the pulsar. After the timing model is made, any deviation we observe from the timing model must be due to some unmodeled effect.

At regular intervals, the North American Nanohertz Observatory for Gravitational Waves (NANOGrav) observes the 49 pulsars that are in the pulsar timing array using the Arecibo Observatory in Puerto Rico and the Green Bank Telescope (GBT) in West Virginia. Such observations allow comparisons to be made between the expected times of arrival and the measured times of arrival. One use of these observations is to improve the timing model for the pulsar. Deviations from the timing model that follow known patterns due to incorrect timing model values can give insight on how to improve the timing model parameters. Thus, the timing model is "self-correcting" in the sense that observations themselves improve the precision of the timing model (see Figure 2).

However, there may be deviations from the timing model that do not correspond to incorrect parameters. These deviations must necessarily, then, come from unmodeled processes. Of the most importance is the deviation corresponding to a sine-like change in the distance between us and the pulsar. Although there could be many potential sources for such a perturbation, a likely candidate is a gravitational wave between the earth and the pulsar. It is possible, however, that such a sine-like signal corresponds to an unmod-

Figure 2: Having an incorrect parameter in the model produces easily detectable and correctable signatures in the residual data [7]. The residuals plotted here represent the magnitude of deviation from the expected time of arrival.

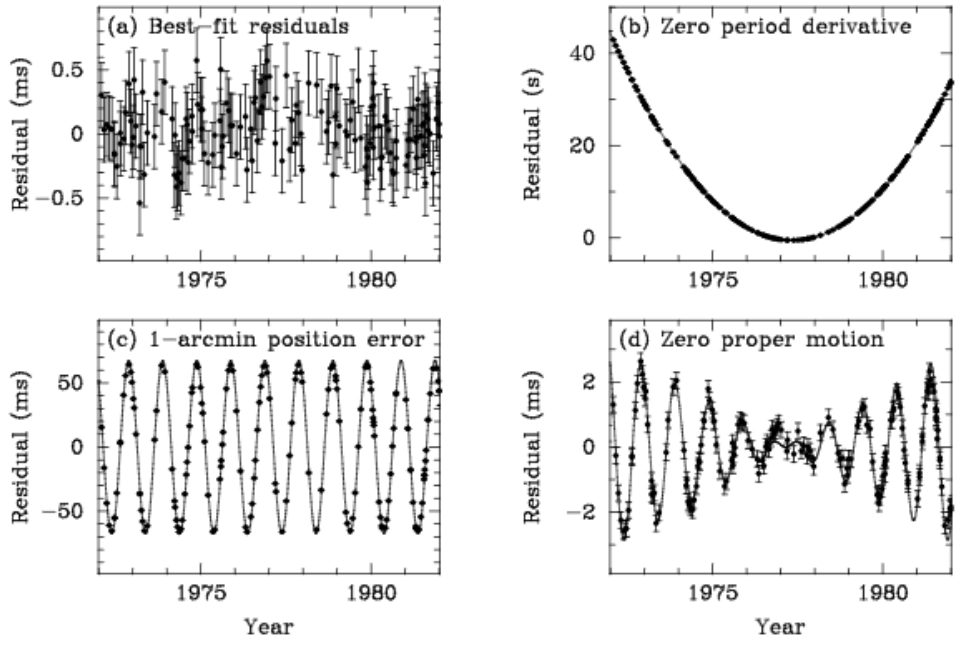

eled process in the timing model. For example, if the pulsar were in a binary system that was not known beforehand, it would appear as if the distance between us and the pulsar were changing sinusoidally because it actually is changing sinusoidally due to the orbit of the pulsar around its companion! Many binary systems have been discovered this way, long before optical telescopes verify the existence of the companion.

To verify whether or not a sine-like signal corresponds to a gravitational wave, the data is searched for a time correlation between pulsars. If the sine wave shows up in multiple pulsars, then it can be concluded that the signal is not originating from an unmodeled process in any individual pulsar. Such a correlated signal must, then, correspond to some unmodeled process in the space between all the pulsars in the galaxy. Using the relative locations of the pulsars, specifics of the sine signal can be probed. Polarity and propagation direction can be ascertained from the relative amplitudes of the signals in the different pulsars in the pulsar timing array.

3 Stochastic Detection

While continuous wave sources are detectable by the PTA, the stochastic background of GWs is what the PTA is best tuned for. The stochastic background of GWs is the sum of all the gravitational waves passing through our galaxy. Dominating the stochastic background is the vast collection of GWs from supermassive black hole binaries. Using the pulsar timing array, the properties of the stochastic background can be probed. This is done by looking for correlated signals across the pulsars, in an analysis similar to the continuous wave search method. By looking for these correlated signals in the data, it is possible to ascertain the relative abundance of the frequencies of waves that contribute to the background. This data can be used, then, to reconstruct population statistics of black hole masses and orbital frequencies in the universe. This gives information on galaxy collision rates, as well as collision duration lengths and galactic black hole masses.

4 High-Frequency Continuous Wave Detection

The International Pulsar Timing Array (IPTA) is a consortium of collaborations from around the world, including NANOGrav in North America, the European Pulsar Timing Array (EPTA) in Europe, and the Parkes Pulsar Timing Array (PPTA) in Australia. The IPTA is tuned to probe GW frequencies in the months-to-years timescale, making it ideal for detecting sources such as supermassive black hole binary systems. Observations of individual pulsars are carried out on a biweekly basis, due to the large number of pulsars that need to be observed. With such infrequent observations, however, GW frequencies on the order of hours remain unexplored. This is due to the intrinsic limit on detection set by the Nyquist frequency, defined as the maximum frequency periodic signal that is detectable for a given sampling frequency. In order to accurately sample a periodic signal, it is necessary to sample at least twice per cycle to avoid introducing errors. Beyond this frequency, the sampling rate is not enough to properly detect a sine wave signal, and any such CW signal would appear as white noise in the data. While large CW sources such as supermassive black hole binary systems do not typically emit CWs at such high frequencies, other exotic emission mechanisms ([3]) have been proposed.

Recently, a 24-hour global observation was carried out on J1713+0747, a particular pulsar, which resulted in a new set of limits on continuous wave (CW) strain in the days to hours frequencies due to the average sampling rate of about 0.5 samples/min [5]. Limits were set for both CW sources in the direction of J1713, as well as random-direction CW sources.

However, J1713 is not the only pulsar that has been observed for long, continuous observations. The pulsars J2302+4442 and J0613–0200 were each observed for multiple hours at a time at the GBT, originally for the purpose of measuring the Shapiro delay effect for each of the pulsars ([8], [6]). Such data sets (see Figures 3 and 4) allow for analysis similar to that done to the J1713 24-hour campaign. These pulsars allow for better directional limits to be placed in the microhertz to millihertz frequency range (Figure 5).

Figure 3: Timing residual plot for the three-hour observation of J0613–0200. Integration time is 120s, and error bars are at the 1-sigma level. Data from four separate sub-bands in the 820MHz band are plotted.

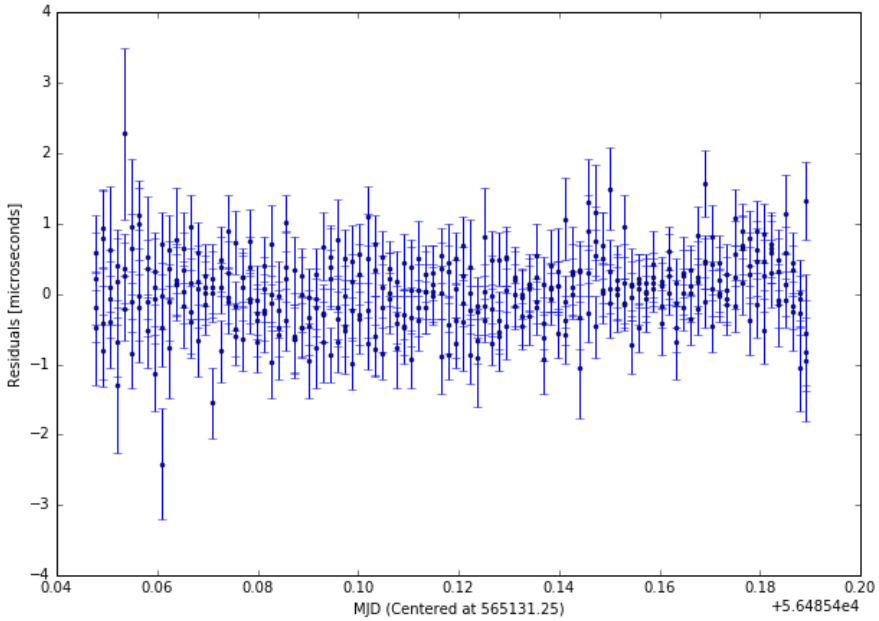

5 Data Used

In 2013, eight pulsars were observed for extended periods of time with the GBT for the initial purpose of observing NANOGrav pulsars with significant Shapiro delays, targeted strategically in order to better observe the delays and therefore improve timing models ([8], [6]). Of the eight data sets, two were chosen for our analysis. Both J2302+4442 and J0613–0200 had small rms residual values, and long continuous timing tracks. Each pulsar was observed three times over the course of the full observation period. For each pulsar, the longest single observation track was selected for observation. J2302 was observed continuously for over 8 hours, and J0613 was observed continuously for over three hours. The residuals were generated using the tempo2 software, drawing its parameters from NANOGrav's 9-year data release. The binary orbit periods of each pulsar are of particular interest, as a

Figure 4: Timing residual plot of the eight-hour observation of J2302+4442. The integration time is 120s, and the error bars are at the 1-sigma level. Data from four separate sub-bands in the 820MHz band are plotted.

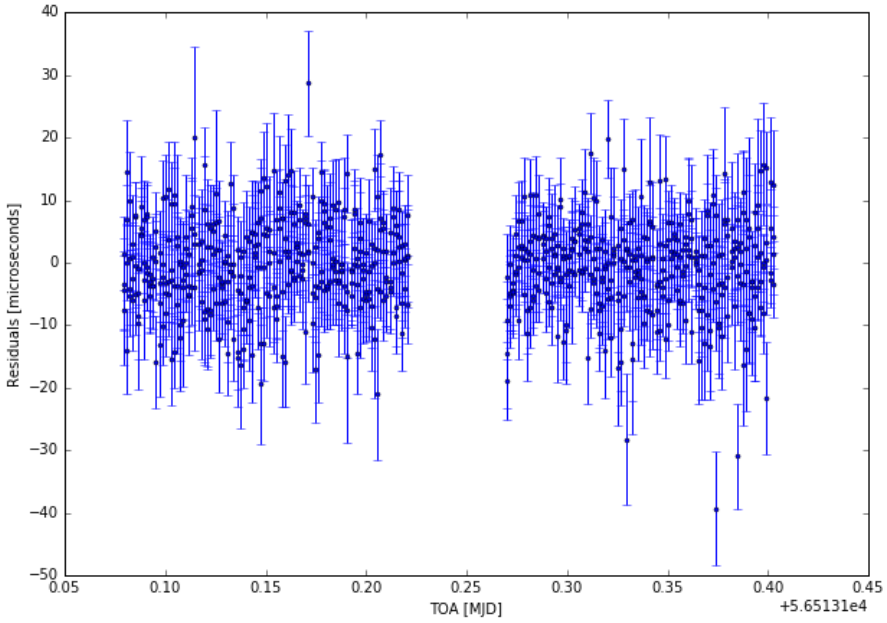

binary period naturally weakens the sensitivity of the pulsar to continuous wave sources of a similar frequency. The binary period for pulsar J2302 is given as about 126 days, and the binary period for pulsar J0613 is given as about 1.2 days.

6 Data Analysis

6.1 Noise

For each pulsar, we developed a noise model to account for any intrinsic or extrinsic sources of noise in the data. The model included both white and red noise estimations. Five parameters were varied: EFAC, EQUAD, Jitter-EQUAD, RN-Amplitude, and RN-Spectral-Index. Using the Markov Chain Monte Carlo method for exploring parameter spaces, we found the maximum

Figure 5: Sky location in RA/DEC of the three pulsars analyzed (J0613–0200, J0645+5158, and J2302+4442), as well as the previously-analyzed J1713+0747. Directional limits are placed in the directions of J2302 and J0645

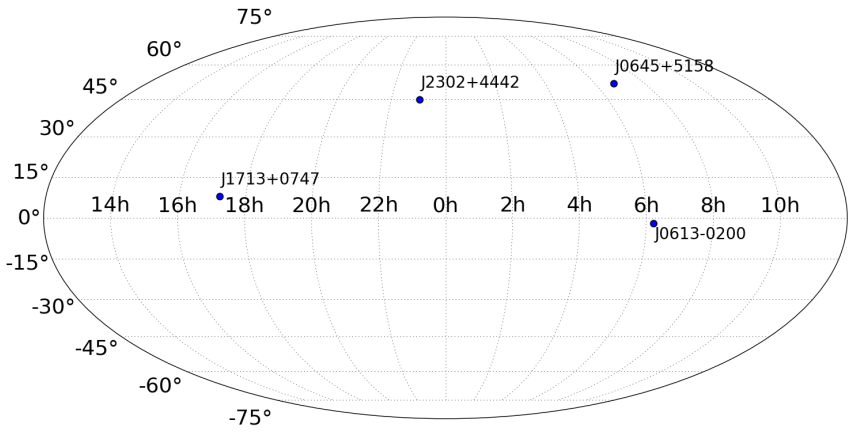

a posteriori values for each parameter, and used them to construct the noise covariance matrix.

The five parameters were chosen for a noise model that has been used in previous analysis schemes. The EFAC parameter acts as a constant multiplier on the TOA uncertainties. The EQUAD parameters represent additional Gaussian white noise added to the EFAC noise. The RN-Amplitude and RN-Spectral-Index parameters describe a red noise variance.

6.2 Detection Statistic

Our main tool for analyzing the sensitivity of a pulsar to continuous wave sources is the F_p statistic ([1]). The F_p statistic is a frequentist detection statistic. It can be thought of as a measure of how much a particular frequency dominates the data. A high F_p statistic is indicative of a potential

Figure 6: The F_p statistic calculated from the residuals. The dashed line shows the minimum F_p value needed to claim a detection with a false alarm probability of 1e-4.

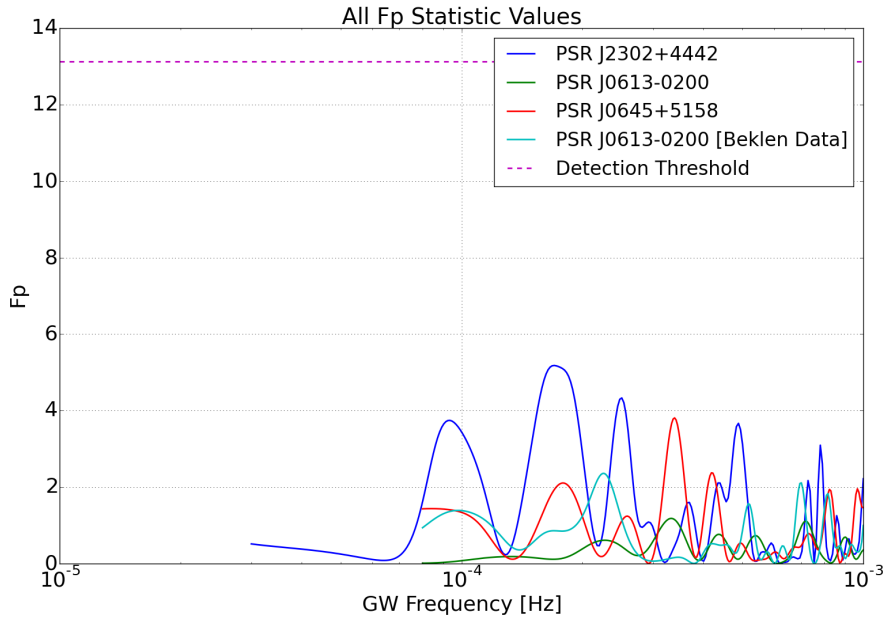

CW source at that frequency. For each potential CW frequency, we calculate the F_p statistic for the data at that frequency. Our detection threshold of about $F_p \geq 13$ corresponds to a false alarm probability of 10^{-4}. That is, the probability of data with an F_p statistic above the minimum value being realized purely by noise (and not a signal) is one in ten thousand.

6.3 Upper Limits and Source Simulation

After creating the noise model for the pulsar, we determine the sensitivity to CW sources at different gravitational wave frequencies. On a high level, this is done by simulating CW sources in random directions with a given strain, and seeing if they can be detected with the given noise model. By ramping up the simulated strain until a detection is made, we obtain the lowest detectable strain–the strain limit–for that GW frequency. To determine whether or not a specific strain can be detected, we simulate 50,000 sources sequentially

in either random directions or, in the case of a directional search, in the direction of the pulsar. Each source is simulated with a random GW emission inclination, and a set distance to keep the strain amplitude constant. Then, for each source, we create simulated residuals based on the CW source and the noise model, and generate an F_p statistic. A source is labelled "detectable" if the F_p statistic is higher than the actual data's F_p statistic. If more than 95% of the simulated sources are detectable, then it can be concluded that a CW source with a strain equal to the fixed strain is detectable above the noise. Thus, that strain is an upper bound on CW source strains for the particular GW frequency being examined.

7 Results

Applying the F_p statistic algorithm to the two pulsars analyzed, we found there was no evidence for a single source gravitational wave signal. However, using the source simulation algorithm, we were able to place upper limits on the strength of the GWs passing through the galaxy at the frequencies probed. Such limits were in coincidence with previously published limits from pulsar J1713+0747. Furthermore, the results coincide with a reasonable extrapolation of the results obtained by NANOGrav and the other PTA consortia.

7.1 Pulsar J0613-0200

Data from the Pennucci campaign ([8]), and the Beklen campaign on PSR J0613-0200 had the smallest average error bars at around 1 microsecond. However, the pulsar is in a binary orbit with period of just over one day, which lies very close to the range of frequencies probed in this study. For this reason, the upper limit curve turns over at low frequencies, as any GW signal could be confounded with an error in the binary period.

Ultimately, the data taken by Beklen had better noise modeling, and produced the lowest omnidirectional limit curve. While this limit curve did not supersede the previously published J1713 limit curve at all frequencies, it lies within an order of magnitude of the J1713 limit.

The precision of the timing of J0613 is reflected in the F_p plot, as J0613 has the smallest F_p statistic, corresponding to more certainty in the non-detection of a signal.

Figure 7: Recent single-source GW limits from the PPTA, EPTA, and NANOGrav, as well as single-pulsar limits from J0437-0745 and B1937+21. Also plotted is the high frequency limits obtained in this analysis from J0613–0200, J0645+5158, and J2302+4442, and the previously published limit from J1713+0747. Here, the data from the Beklen campaign was used for J0613

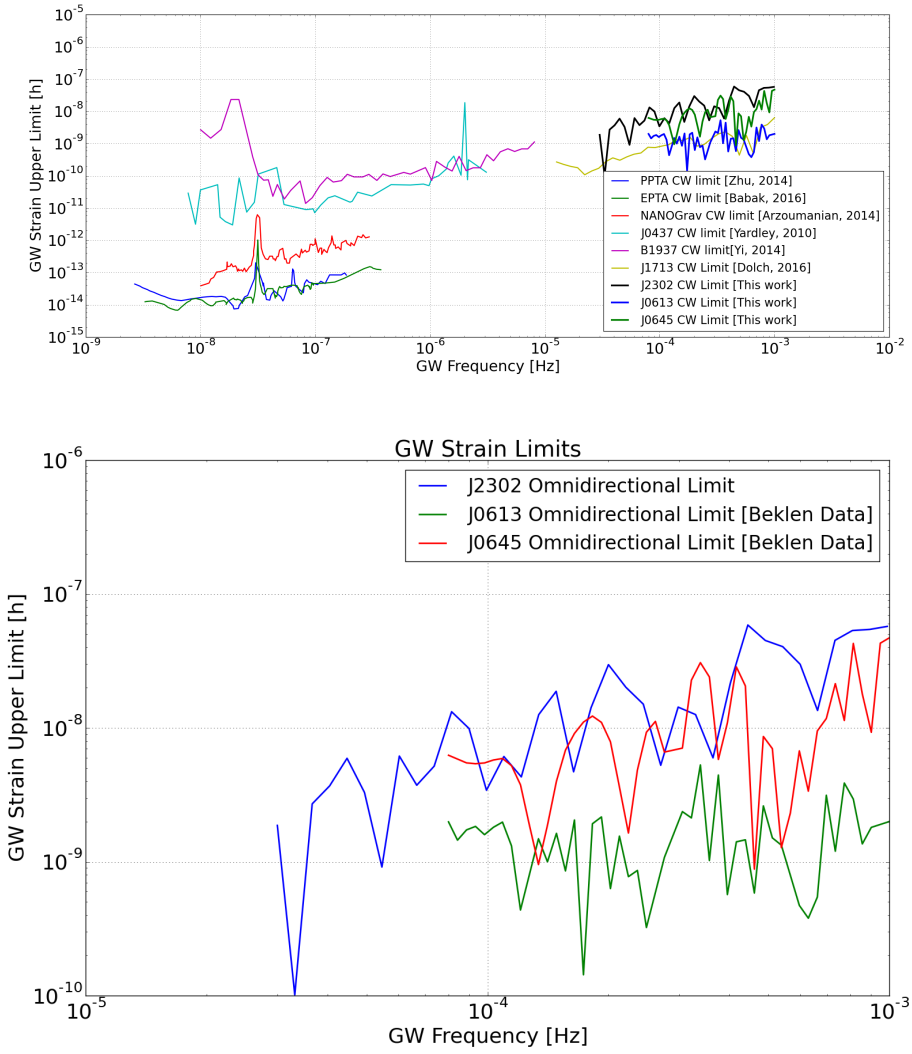

7.2 Pulsar J0645+5158

Pulsar J0645+5158 was observed by Elif Beklen on the Green Bank telescope, and offers the best limits in both the omnidirectional and directional cases. Since J0645 is not in a binary system, we do not have the same problem that J0613 has with binary period conflation. However, due to larger error bars, J0645 was not able to match J0613 in the omnidirectional limit curve.

However, J0645 was able to produce the best directional limit curve. The directional limit was about one order of magnitude lower than the omnidirectional limit, which matches with the behavior of the J1713 omnidirectional and directional limits.

An interesting feature of the J0645 data lies in the structure of the low-frequency limit curve. Certain features, such as the parabolic sweep near the tail end, appear in both the directional and omnidirectional limit curves. This suggests some structure to the residuals that may have been unaccounted for in the noise modeling. Such structure is not explored in this work, but may be the topic of study for future work.

7.3 Pulsar J2302+4442

Pulsar J2302+4442 was observed in the Pennucci campaign, and is the longest data set analyzed. The campaign took data for eight hours, which allows analysis for detection of GWs at periods up to eight hours in length. For this reason, J2302 provides the most comprehensive limit, extending almost an order of magnitude in frequency beyond the other pulsars analyzed.

J2302 also provided good directional limits, which again were consistently about an order of magnitude below the corresponding directional limit.

8 Conclusion

Using our pipeline, we were able to recreate the omnidirecitonal limits from the J1713 24-hour global campaign, which verified the integrity of our analysis algorithm. Using data from the Green Bank Telescope taken by Tim Pennucci and Elif Beklen on puslars J0613-0200, J0645+5158, and J2302+4442, we were able to place omnidirectional limits consistent with limits already placed in that GW frequency range. Furthermore, directional limits in the direction of pulsars J0645 and J2302 were placed, which limited GW strains by an additional order of magnitude in these directions.

Figure 8: Directional limits established in the direction of J2302 and J0645. Also plotted is the J0613 directional limit from the Beklen campaign, which was significantly higher than expected.

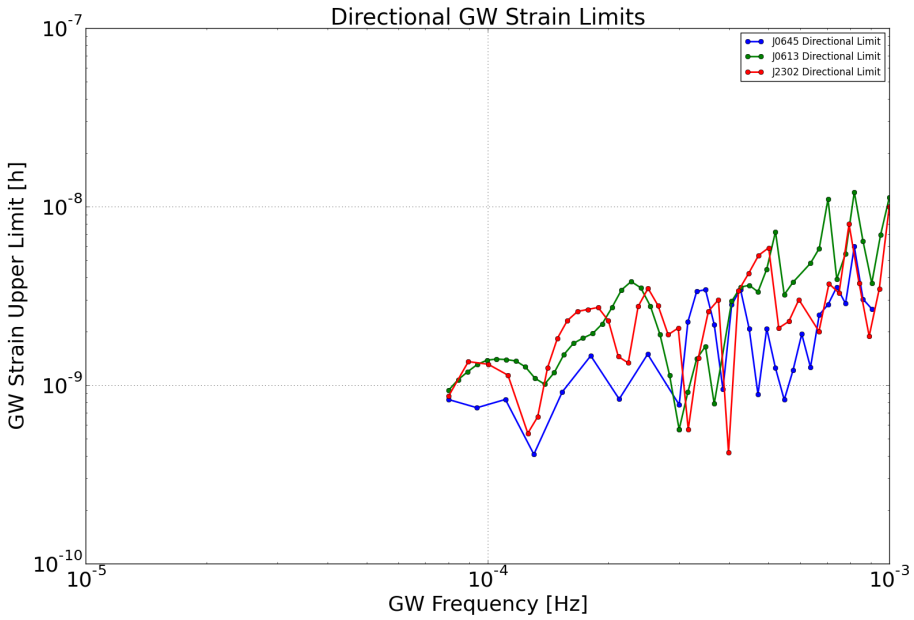

Further analysis will attempt to remove statistical fluctuations in the data through using a greater amount of simulations. Furthermore, the noise model can be improved upon by sampling the parameter space of the noise model more precisely. Also, similar analyses can be carried out on each of the other pulsars observed in the two projects. For each pulsar, strict directional limits on CW strain amplitude can be placed for GW frequencies in the microhertz to millihertz range.

The directional limit curve for J0613 did not follow the pattern of being reduced by an order of magnitude. Instead, the directional limit was worse than the omnidirectional limit. This result is very surprising, and indicates a problem in the noise model for J0613. Further study of the noise model for this pulsar will shed light onto the nature of this discrepancy.

This method, however, is not the only way to probe the microhertz to millihertz frequency range. The Laser Interferometer Space Antenna (LISA) will be sensitive to these frequencies as well, and will have much better sensitivity. However, the lines-of-sight of LISA will be very localized (1000km) compared to the lines-of-sight of the PTA, which extend across the galaxy. For this reason, PTAs are very sensitive to galactic-source objects that may fall in a line-of-sight. In this scenario, the apparent strain for the PTA will be much larger than the apparent strain for LISA, and the PTA will have a better chance at detecting these sorts of sources. Work is being done to modify the PTA analysis for intragalactic source detection and limit generation, but such calculations require strong-field relativity, which is much more difficult to work with.

Appendix A

Step-By-Step Instructions for Data Analysis of Long-Track Data for High Frequency GW Detection

What you'll need: -computer with linux installed (could potentially work on mac as well)

Installing tempo2

Tempo2 can be found at `https://bitbucket.org/psrsoft/tempo2`, or grabbed by using the command

```
git clone https://bitbucket.org/psrsoft/tempo2.git
```

After getting all the files, follow the instructions included in the README. [Plugins like plk (the graphics interface that uses PGPLOT) are not necessary for data analysis, but can be useful to visualize your data before analysis. However, installation of PGPLOT and plk is not covered in this manual.]

The command ./configure will attempt to configure all compilers and plugins to get ready for the make. Any errors you might have will come up in this step. Note, if you would like to install tempo2 in a particular location aside from the default, use the command

```
./configure --prefix=/your/install/path
```

If you are getting an error regarding your gcc and F77: Make sure you have compilers for c and fortran installed, since tempo2 requires both of them. Furthermore, they need to be able to cross link. Some versions of F77, for example, do not cross link with other versions of gcc. Therefore, it is best to use gcc and gfortran to compile tempo2. If `./configure` is still looking at F77 instead of gfortran, run the command

```
export F77=gfortran
```

Which will set your fortran compiler to gfortran manually. Then, run `./configure` again to pick up the changes.

Once `./configure` passes, the environment is set up to run make correctly. Running the command

```
make && make install
```

will compile all the necessary components. Note, you may have to run as su, as make creates some new directories.

That's it! You can run make clean to delete the unnecessary files from installation, and you can run `make plugins && make install plugins` to install the relevant plugins.

If everything worked successfully, there should now be a program called tempo2 that is runnable from the command line. Running

```
tempo2 -v
```

will verify that tempo2 is correctly installed.

Installing PAL2

Luckily, PAL2 is significantly easier to install than tempo2. First, clone the git repo with the command

```
git clone https://github.com/jellis18/PAL2.git
```

Second, you'll want to grab an environment manager like Anaconda (`https://docs.continuum.io/anaconda/install`) to manage the python packages that PAL2 needs. After installing anaconda, run the command

```
conda env create -f environment.yml
```

which will create an environment called `pal2_conda` based off the dependencies in `environment.yml`. Note, if there are issues with certain versions not being available for your OS, use the command

```
conda search \$PACKAGE
```

where `$PACKAGE` is the package name that has an incompatible version, and find the version number that is closest to the one `environment.yml` wants. Then, edit `environment.yml` to the version numbers that work.

After conda creates the environment, switch to it with

```
source activate pal2\_conda
```

Next, proceed with the installations that conda does not handle with the commands

```
pip install -r requirements.txt
pip install libstempo --install-option="--with-tempo2=\$TEMPO2"
```

and run

```
python setup.py install
```

If everything worked successfully, the scripts `makeh5File.py` and `PAL2_run.py` should be executable. Check this with:

```
./PAL2\_run.py -h
```

If the installation was successful, the script should return a long list of options that are available.

Generating an hdf5 file

In order to properly process the data from a .par and .tim file, it must first be put into a format that PAL2 can handle. The hdf5 format (Hierarchical Data Format 5) was chosen as the data model to store the relevant data from the .par and .tim files. In order to convert raw data into an hdf5 data model, the data must first be consolidated into a single .tim file with a single .par file to go with it. The .par should have fits turned on for FD parameters, as well as DM and F0. Put the .tim file in a subdirectory (usually `./tim/`) and the .par file in a different subdirectory (usually `./par/`). Then, run the `makeH5File.py` script that came packaged with PAL2.

```
makeH5File.py --pardir "./par/" --timdir "./tim/"
--h5File "name\_of\_output.hdf5"
```

If everything worked successfully, there should now be a file called `"name_of_output.hdf5"` in the current directory. This is the file to send to the upper limit script.

Generating Noise

In order to correctly run simulations based on the data, a proper noise model must be established. This is done by exploring the noise model parameter space (usually a five-dimensional space) using a Markov Chain Monte Carlo algorithm to maximize the likelihood that a particular combination of parameters models the noise correctly. To run the algorithm, invoke the `PAL2_run` script with:

```
PAL2\_run.py --h5File "/path/to/h5File.hdf5" --outDir
"/path/to/output/directory/" --nf 30 --incEquad --incJitterEquad
--mark6 --pulsar <pulsar name>
```

The additional parameter `--incRed` will include two additional parameters for modelling red noise, but may not be necessary for short data sets.

If everything worked successfully, there should now be a directory with the noise data stored in multiple .txt files. The specific format of the noise subdirectory is not important, as the upper limit script knows how to deal with it.

Generating an Upper Limit

Once the noise model is built correctly, the final step is to run the suite of simulations in the `generateUpperLimit.py` file for the data and noise model. This can be done by running the command:

```
generateUpperLimits.py --file /path/to/hdf5File.hdf5
--noise-dir /path/to/noise/ --out-dir /path/to/output/directory/
--psr <pulsar name> --frq-resolution 50 --nreal 10000
--run-name <descriptive simulation name>}
```

The parameter `--frq-resolution` can be changed to sample the frequency window more or less depending on how resolved you need the limit curve to be. The parameter `--nreal` controls the number of realizations (or simulations) done per upper limit. It should be no less than 10000, and in practice should be a lot more than that.

The script will output its results per-frequency to stdout, as well as to a text file that it will generate and save in the `--out-dir`.

If everything worked successfully, there should now be a numpy-compatible .txt file with the generated upper limit on CW strain in the frequency range specified in `generateUpperLimit.py`!

References

[1] Z. Arzoumanian, A. Brazier, S. Burke-Spolaor, S. J. Chamberlin, S. Chatterjee, J. M. Cordes, P. B. Demorest, X. Deng, T. Dolch, J. A. Ellis, R. D. Ferdman, N. Garver-Daniels, F. Jenet, G. Jones, V. M. Kaspi, M. Koop, M. T. Lam, T. J. W. Lazio, A. N. Lommen, D. R. Lorimer, J. Luo, R. S. Lynch, D. R. Madison, M. A. McLaughlin, S. T. McWilliams, D. J. Nice, N. Palliyaguru, T. T. Pennucci, S. M. Ransom, A. Sesana, X. Siemens, I. H. Stairs, D. R. Stinebring, K. Stovall, J. Swiggum, M. Vallisneri, R. van Haasteren, Y. Wang, W. W. Zhu, and NANOGrav Collaboration. Gravitational Waves from Individual Supermassive Black Hole Binaries in Circular Orbits: Limits from the North American Nanohertz Observatory for Gravitational Waves. *Astrphysical Journal*, 794:141, Oct. 2014.

[2] S. Babak, A. Petiteau, A. Sesana, P. Brem, P. A. Rosado, S. R. Taylor, A. Lassus, J. W. T. Hessels, C. G. Bassa, M. Burgay, R. N. Caballero, D. J. Champion, I. Cognard, G. Desvignes, J. R. Gair, L. Guillemot, G. H. Janssen, R. Karuppusamy, M. Kramer, P. Lazarus, K. J. Lee, L. Lentati, K. Liu, C. M. F. Mingarelli, S. Osłowski, D. Perrodin, A. Possenti, M. B. Purver, S. Sanidas, R. Smits, B. Stappers, G. Theureau, C. Tiburzi, R. van Haasteren, A. Vecchio, and J. P. W. Verbiest. European Pulsar Timing Array limits on continuous gravitational waves from individual supermassive black hole binaries. *Monthly Notices of the Royal Astronomical Society*, 455:1665–1679, Jan. 2016.

[3] D. F. Chernoff. Clustering of superstring loops. *ArXiv*, 2009.

[4] C. Cutler, S. Burke-Spolaor, M. Vallisneri, J. Lazio, and W. Majid. The gravitational-wave discovery space of pulsar timing arrays. *Phys. Rev. D*, 89:042003, Feb 2014.

[5] T. Dolch, N. Collaboration, J. A. Ellis, S. Chatterjee, J. M. Cordes, M. T. Lam, C. Bassa, B. Bhattacharyya, D. J. Champion, I. Cognard, K. Crowter, P. B. Demorest, J. W. T. Hessels, G. Janssen, F. A. Jenet, G. Jones, C. Jordan, R. Karuppusamy, M. Keith, V. I. Kondratiev, M. Kramer, P. Lazarus, T. J. W. Lazio, D. R. Lorimer, D. R. Madison, M. A. McLaughlin, N. Palliyaguru, D. Perrodin, S. M. Ransom, J. Roy, R. M. Shannon, R. Smits, I. H. Stairs, B. W. Stappers, D. R. Stinebring,

K. Stovall, J. P. W. Verbiest, and W. W. Zhu. Single-source gravitational wave limits from the j1713+0747 24-hr global campaign. *Journal of Physics: Conference Series*, 716(1):012014, 2016.

[6] E. Fonseca, T. T. Pennucci, J. A. Ellis, I. H. Stairs, D. J. Nice, S. M. Ransom, P. B. Demorest, Z. Arzoumanian, K. Crowter, T. Dolch, R. D. Ferdman, M. E. Gonzalez, G. Jones, M. L. Jones, M. T. Lam, L. Levin, M. A. McLaughlin, K. Stovall, J. K. Swiggum, and W. Zhu. The NANOGrav Nine-year Data Set: Mass and Geometric Measurements of Binary Millisecond Pulsars. *Astrphysical Journal*, 832:167, Dec. 2016.

[7] D. R. Lorimer. Binary and Millisecond Pulsars. *Living Reviews in Relativity*, 11, Nov. 2008.

[8] T. Pennucci. *Wideband Observations of Radio Pulsars*. PhD thesis, 2015.

[9] D. R. B. Yardley, G. B. Hobbs, F. A. Jenet, J. P. W. Verbiest, Z. L. Wen, R. N. Manchester, W. A. Coles, W. van Straten, M. Bailes, N. D. R. Bhat, S. Burke-Spolaor, D. J. Champion, A. W. Hotan, and J. M. Sarkissian. The sensitivity of the Parkes Pulsar Timing Array to individual sources of gravitational waves. *Monthly Notices of the Royal Astronomical Society*, 407:669–680, Sept. 2010.

[10] S. Yi, B. W. Stappers, S. A. Sanidas, C. G. Bassa, G. H. Janssen, A. G. Lyne, M. Kramer, and S.-N. Zhang. Limits on the strength of individual gravitational wave sources using high-cadence observations of PSR B1937+21. *Monthly Notices of the Royal Astronomical Society*, 445:1245–1252, Dec. 2014.

[11] X.-J. Zhu, G. Hobbs, L. Wen, W. A. Coles, J.-B. Wang, R. M. Shannon, R. N. Manchester, M. Bailes, N. D. R. Bhat, S. Burke-Spolaor, S. Dai, M. J. Keith, M. Kerr, Y. Levin, D. R. Madison, S. Osłowski, V. Ravi, L. Toomey, and W. van Straten. An all-sky search for continuous gravitational waves in the Parkes Pulsar Timing Array data set. *Monthly Notices of the Royal Astronomical Society*, 444:3709–3720, Nov. 2014.